

Article

# Oxidation of Phospholipids by OH Radical Coordinated to Copper Amyloid- $\beta$ Peptide—A Density Functional Theory Modeling <sup>†</sup>

Alberto Rovetta, Laura Carosella, Federica Arrigoni, Jacopo Vertemara , Luca De Gioia, Giuseppe Zampella and Luca Bertini \* 

Department of Biotechnologies and Biosciences, University of Milano-Bicocca, Piazza della Scienza 2, 20126 Milan, Italy

\* Correspondence: luca.bertini@unimib.it

<sup>†</sup> This paper is dedicated to Professor Wolfgang Weigand on the occasion of his 65th birthday.

**Abstract:** Oxidative stress and metal dyshomeostasis are considered crucial factors in the pathogenesis of Alzheimer's disease (AD). Indeed, transition metal ions such as Cu(II) can generate reactive oxygen species (ROS) via O<sub>2</sub> Fenton-like reduction, catalyzed by Cu(II) coordinated to the amyloid-beta (A $\beta$ ) peptide. Despite intensive efforts, the mechanisms of ROS-induced molecular damage remain poorly understood. In the present paper, we investigate, on the basis of Density Functional Theory (DFT) computations, a possible mechanism of the OH radical propagation toward membrane phospholipid polar head and fatty acid chains starting from the end-product of the OH radical generation by Cu(II)-A $\beta$ . Using phosphatidylcholine as a model of a single unit inside a membrane, we evaluated the thermochemistry of the OH propagation with the oxidation of a C-H bond and the formation of the radical moiety. The DFT results show that Cu(II)-A $\beta$ -OH can oxidize only sn-2 C-H bonds of the polar head and can easily oxidize the C-H bond adjacent to the carbon-carbon double bond in a mono or bis unsaturated fatty acid chain. These results are discussed on the basis of the recent literature on in vitro A $\beta$  metal-catalyzed oxidation and on the possible implications in the AD oxidative stress mechanism.

**Keywords:** copper amyloid peptide; Alzheimer's disease; oxidative stress; CuA $\beta$  hypothesis; phospholipid membrane; Density Functional Theory; molecular modeling



**Citation:** Rovetta, A.; Carosella, L.; Arrigoni, F.; Vertemara, J.; De Gioia, L.; Zampella, G.; Bertini, L. Oxidation of Phospholipids by OH Radical Coordinated to Copper Amyloid- $\beta$  Peptide—A Density Functional Theory Modeling. *Inorganics* **2023**, *11*, 227. <https://doi.org/10.3390/inorganics11060227>

Academic Editors: Christelle Hureau, Ana Maria Da Costa Ferreira, Gianella Facchin and Vladimir Arion

Received: 2 March 2023

Revised: 26 April 2023

Accepted: 22 May 2023

Published: 25 May 2023



**Copyright:** © 2023 by the authors. Licensee MDPI, Basel, Switzerland. This article is an open access article distributed under the terms and conditions of the Creative Commons Attribution (CC BY) license (<https://creativecommons.org/licenses/by/4.0/>).

## 1. Introduction

Alzheimer's disease (AD) is the most common form of dementia that contributes to 60–70% of cases of dementia in the elderly. Among the numerous data reported in the annual 2022 Alzheimer's disease facts and figures [1] drafted by the U.S. non-profit Alzheimer's Association, there is one that is particularly striking: it is estimated that there are 6.5 million Americans living with AD, which could grow up to 13.8 million in 2060; this is equivalent to the population of the U.S. state of Pennsylvania (Census.gov). This compelling data highlight the need for a therapeutic approach to AD since one is sadly still lacking.

AD is a multifactorial disorder characterized by several features such as deposits of senile plaques, hyperphosphorylated tau protein, and extensive synaptic/neuronal loss. Since its publication in 1992, the amyloid cascade hypothesis [2] became dominant in the description of AD pathogenesis and has driven drug development. It postulates that amyloid-beta (A $\beta$ ) peptide, a 39–42-residue peptide that comes from the amyloidogenic proteolytic cleavage of the neuronal APP membrane protein, and triggers neuron impairment and death in a variety of forms. Over the years, intense research activity has proposed several therapeutic strategies whose clinical trials have not been successful, as in the case of one of the anti-beta amyloid monoclonal antibodies recently tested [3]. These facts

have further highlighted the need to broaden the perspective of the amyloid hypothesis alone [4–7].

It is well established that, within the multifactorial nature of AD, one of the major histopathological hallmarks is the presence of amyloid senile plaques, which are large extracellular aggregates of the A $\beta$ . Prompted by the stabilization of a misfolded hairpin form of A $\beta$  [8], small A $\beta$  oligomers [9–11] are formed, which subsequently further aggregate to fibrils and finally plaques.

There are two important pieces of experimental evidence in defining what has been recently named the CuAD hypothesis [12], i.e., alterations in copper homeostasis [13–20] and the oxidative stress observed in post-mortem AD brain tissue [21,22]. In particular, copper ions could induce oxidative stress, giving rise to lively research work that goes from mechanistic studies [23–26] to the design of pharmacological strategies [15–17,27].

There is a large body of evidence that copper binds A $\beta$  peptide [13,14,25–28] and that Cu(II)-A $\beta$  species are redox-active [29]. In vitro and in the presence of molecular oxygen and a reducing agent such as ascorbate, Cu(II)-A $\beta$  can be a direct source of reactive oxygen species (ROS) [30,31]. The mechanism is a three-step Fenton-like process in which the redox cycling of Cu(II)-A $\beta$ /Cu(I)-A $\beta$  in aerobic conditions results in the production of superoxide [32], hydrogen peroxide [33], and the highly reactive hydroxyl radical [34]. These ROS can further propagate toward the biological substrates, inducing oxidative stress through lipid peroxidation, nucleic acid [35], and protein oxidation [36] in the AD brain [37–39]. The in silico modeling approach has given an important contribution in revealing the active molecular mechanisms that drive AD [11,40,41], particularly including those related to Cu/A $\beta$  interactions.

The complete mechanism of ROS production was also investigated in our laboratory using quantum chemistry and molecular modeling tools, since most of the species involved are transiently populated and thus difficult to detect at a spectroscopical level. Following the approach of Giacobazzi et al. [42], we investigated, at the Density Functional Theory [43–45] level (DFT), the mechanism of O<sub>2</sub> reduction assisted by the Cu(II)-A $\beta$ (1-2) model system in the presence of ascorbate as a reducing agent.

The scheme of this mechanism is depicted in Figure 1. Briefly, the first step of this process (Figure 1, green) is also the rate-determining one: Cu(II)-A $\beta$  undergoes reduction to Cu(I) by one equivalent of ascorbate and successively binds one O<sub>2</sub> molecule, which is the slow endergonic step (free energy barrier around 24.8 kcal/mol [44]). At this point, superoxide is formed and can eventually leave the Cu(II) coordination sphere (Figure 1, blue). The two next steps (Figure 1, yellow) are both exergonic, with the formation of the hydroperoxide HO<sub>2</sub><sup>−</sup> and the hydroxyl anion plus a hydroxyl radical. In this Cu(II)-A $\beta$ -OH form (vide infra), the OH radical is coordinated to copper and can propagate, inducing oxidative stress at the cellular level. We estimated a standard reduction potential of the couple Cu(II)-A $\beta$ -OH/Cu(II)-A $\beta$ -OH<sup>−</sup> of 1.4 V, which results in roughly 1.3 V less oxidating than free solvated OH radical (OH/OH<sup>−</sup> 2.73 V) [45].

At this point, a question arises spontaneously: is this Cu(II)-A $\beta$ -OH form able to induce oxidative stress by propagating the OH radical toward phospholipid membranes? The purpose of this paper is to attempt to answer this question through DFT calculation by using the same approach recently adopted to investigate amino acid oxidation [46]. In the following, starting from the Cu(II)-A $\beta$ -OH form [45], we investigate its binding and the OH propagation toward a phosphatidylcholine single molecule, focusing on either the propagation toward the dipolar head group or the aliphatic chain of selected fatty acids.

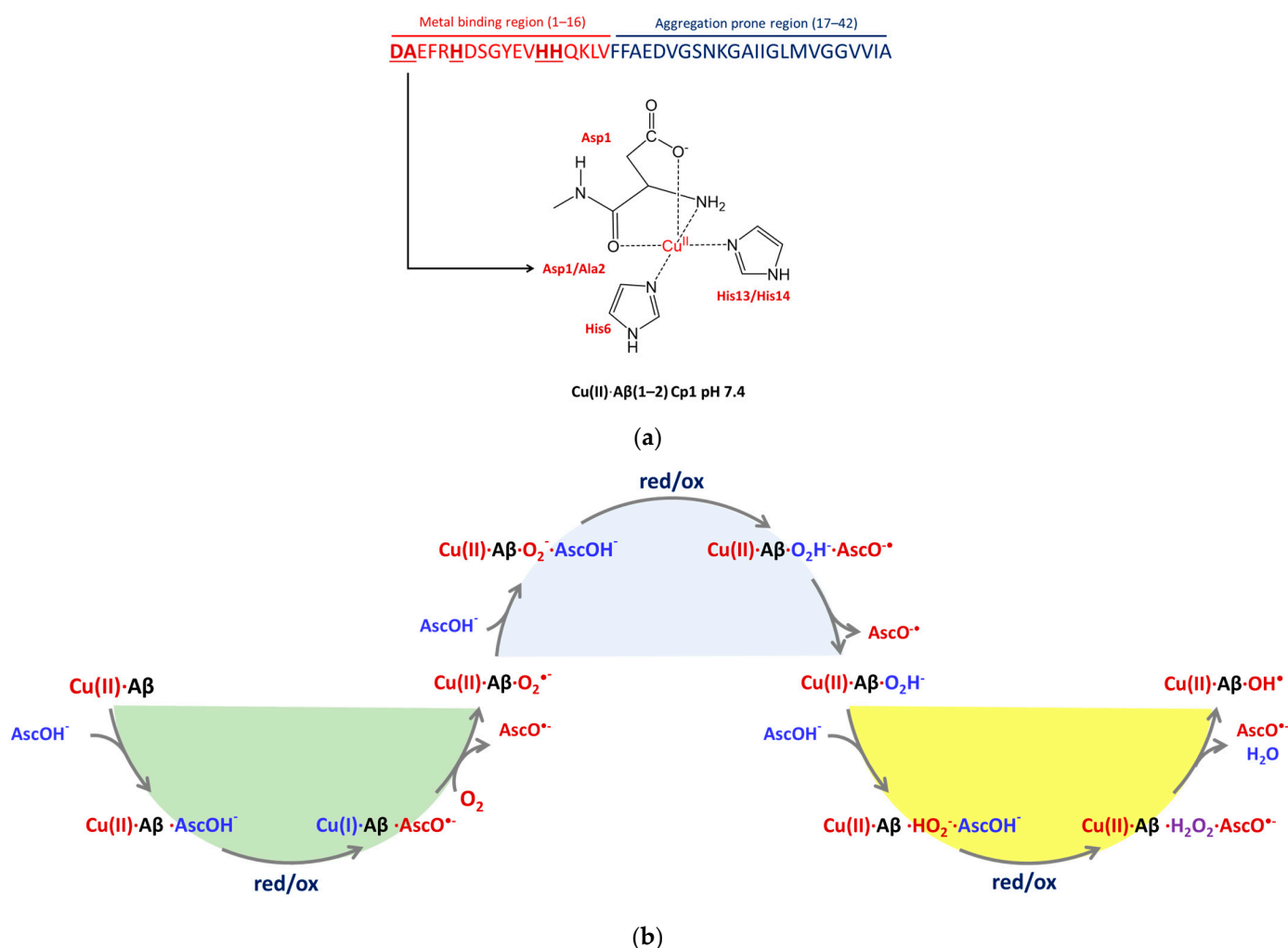


**Figure 1.** (a) Structure of the pH 7.4 Component 1 (Cp1) Cu(II)-Aβ(1-2) investigated in Refs. [43–45]. In the Aβ primary structures, the metal binding region is evidenced (in red), with the three His residues that are involved in the Cu(II) binding. (b) Scheme of the three-step Fenton-like O<sub>2</sub> reduction mechanism by ascorbate (AscOH<sup>-</sup>) assisted by Cu(II)-Aβ.

## 2. Results

### 2.1. The Electronic Structure of Cu(II)-Aβ-OH

The molecular shape and the electronic structure of the Cu(II)-Aβ-OH investigated in Ref. [45] are peculiar. The Cu(II) coordination includes, in addition to the Asp1 side chain and the amino terminal, two OH ligands; formally, one is a radical and the other is an OH-anion (Figure 2). In the five-coordinated form, the apical ligand can be an imidazole ring of histidine residues. The electronic structure can be described as follows. The electron vacancy that defines the nature of the OH radical is delocalized over the two oxygen atoms that belong to the OH groups and on the amino terminal with the formation of an amino radical species (see Figure 2A). In addition, the Cu(II) d<sup>9</sup> couples with the unpaired electron on the three centers, which results in a global Cu(II)-Aβ-OH singlet ground state (Figure 2B) according to DFT Natural Bond Orbitals (NBO) atomic and spin populations. This result implies that roughly one-third of the 1e vacancy is delocalized on each of the three ligands. This fact is nicely put in evidence by the frontier MOs reported in Figure 2C, which are those that mix, in a bonding way, the Cu(II) d orbitals with p orbitals on oxygen and nitrogen atoms. For these reasons, the oxidizing power of this species is less than free-solvated OH by 1.3 V [45].

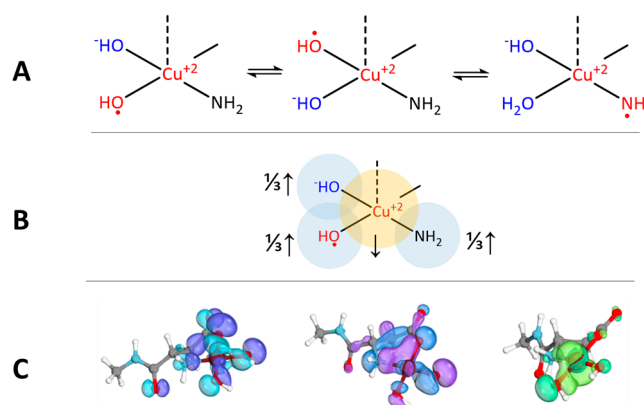


**Figure 2.** (A) Structure of the Cu(II) coordination in Cu(II)-A $\beta$ -OH, evidencing that the negative charge (in blue) and the electron vacancy (in red) can be delocalized on three centers; (B) scheme of  $S = 0$  Cu(II)-A $\beta$ -OH electronic structure ground state; (C) frontier MOs (cutoff 0.05 a.u.) that describe the delocalization as described in (A,B).

To further investigate the structure of the Cu(II)-A $\beta$ -OH species, we carried out a DFT conformational sampling on the Cu(II)-A $\beta$ (1-7)(OH) $_2^-$  (Figure 3), where as many as three charged residues are found. Moreover, these computations will allow us to compute the binding energy between Cu(II)-A $\beta$ -OH and phosphatidylcholine moiety. The details of this conformational search are reported in the Supplementary Materials.

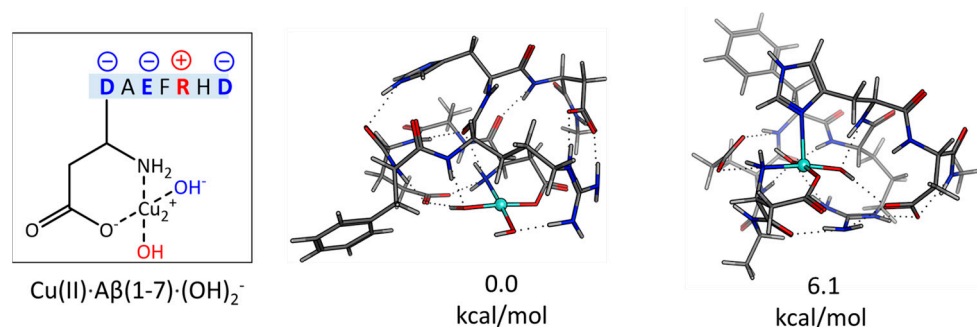


**Figure 3.** Left: Cu(II)-A $\beta$ (1-7)(OH) $_2^-$  model in which charged residues are evidenced. Right: Most stable 4-coordinated and 5-coordinated forms identified upon DFT speciation. The energy difference is computed (in kcal/mol) with respect to the 4-coordinated form which is also the most stable of all those identified. The dotted lines evidence the H-bonding network.

According to this DFT speciation study, (a) the lowest energy form has the two OH groups in the cis position with respect to Cu(II); (b) the lowest energy form is four-coordinated; (c) the most stable five-coordinated form is 6.1 kcal/mol higher in energy with the His6 imidazole ring that occupies the Cu(II) apical position. It is interesting that most of the low-energy forms are characterized by Arg5/Glu3 or Arg5/Asp7 salt bridges.

## 2.2. Cu(II)-A $\beta$ -OH Propagation Mechanism

In this paper, we investigated the radical propagation of Cu(II)-A $\beta$ -OH toward the C-H bonds that belong to methyl and methylene groups of phospholipid polar head and fatty acid chains. In general, this is a spin-forbidden hydrogen abstraction process, as sketched in Figure 4.

Starting from Cu(II)-A $\beta$ -OH/substrate adduct, the  $S = 0$  singlet potential energy surface (PES) along the C-H bond elongation coordinate, which describes the radical propagation, crosses the  $S = 1$  triplet PES. The molecular structure at this  $S = 0/S = 1$  crossing point can be considered the transition state of the process. By continuing to lengthen the C-H distance, the energy of the system decreases, reaching the  $S = 1$  final

product in which one unpaired electron is localized at the aliphatic carbon atom under OH attack and one is at the Cu(II) center.

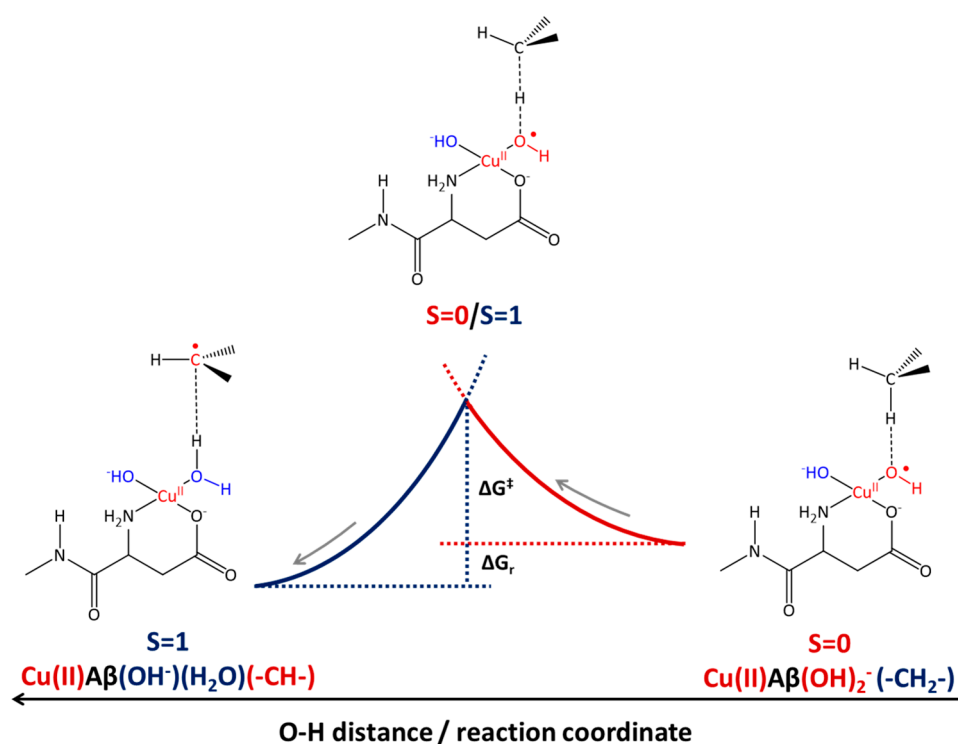


**Figure 4.** General trend of the singlet- and triplet-state PESs along the O–H reaction coordinate that describes the hydrogen abstraction from a methylene group (that belongs to the polar head or to the aliphatic chain) to the OH of Cu(II)-Aβ-OH coordination. Starting from S = 0 state, upon OH propagation, the electron vacancy is shifted on the carbon radical, resulting in a final product with triplet ground state. The structure at the crossing between S = 0 and S = 1 PES represents the transition state of the process.

### 2.3. Phosphatidylcholine Moiety, Structure, and Reactivity toward Cu(II)-Aβ-OH

In this section, we explore the reactivity of Cu(II)-Aβ-OH toward a phosphatidylcholine (PC) model (see Figure 5) with two acetyl groups instead of the fatty acid aliphatic chains.

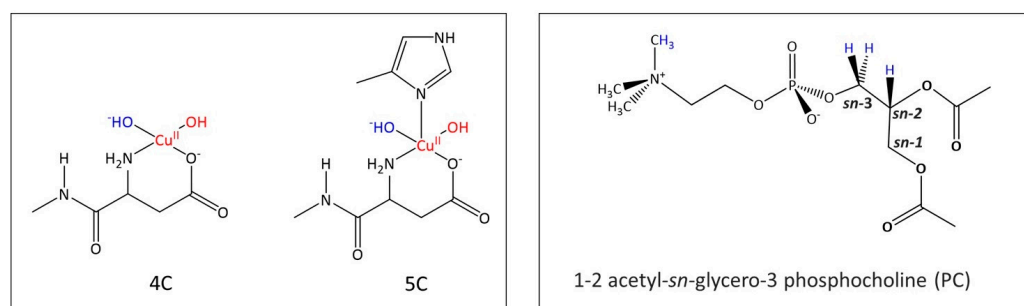
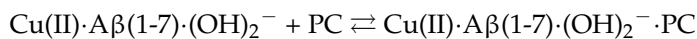


**Figure 5.** **Left:** Four- and five-coordinated Cu(II)-Aβ-(OH)<sub>2</sub>•<sup>-</sup> models considered in this paper. Model 5C has one imidazole ring bound to Cu(II) in the apical position which is derived from one of the histidine residues of Aβ peptide (very likely His6). **Right:** The phosphatidylcholine (PC) model used to explore the Cu(II)-Aβ-(OH)<sub>2</sub>•<sup>-</sup> propagation toward the polar head of membranes. In the PC structure, the possible C-H bonds oxidized by OH radical are evidenced in blue (“sn” = stereospecifically numbered): the methyl group of the quaternary ammonium of the choline portion, and the CH<sub>2</sub> and CH in the sn-2 and sn-3 positions of the glycerol portion.

We evaluate the binding between PC and Cu(II)-A $\beta$ -OH (Figure 6A) starting from the Cu(II)-A $\beta$ (1-7)(OH) $_2^-$  model coordination already presented above according to the following equation:



and considering the total binding energy for 63 different structures (Figure 6B, see Supplementary Materials for details on the conformational search approach).

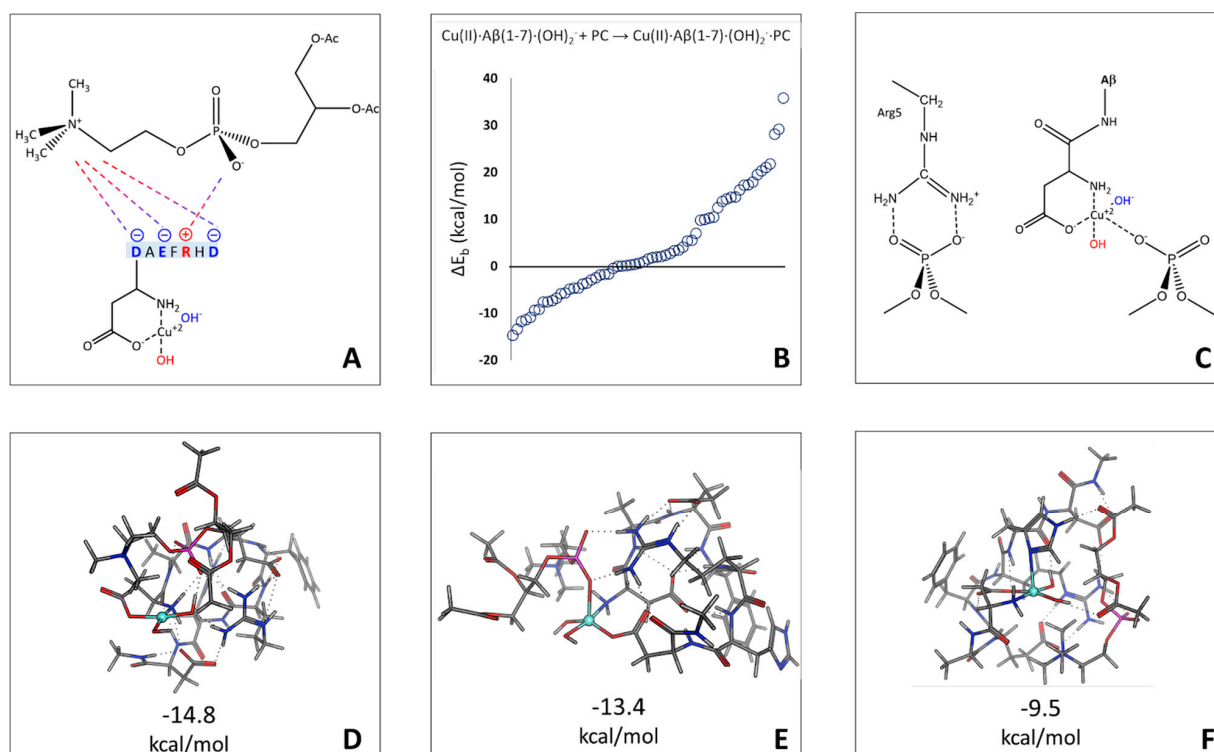


**Figure 6.** (A) Model adopted for the Cu(II)-A $\beta$ (1-7)(OH) $_2^-$ ·PC interaction; (B) total binding energy (in kcal/mol) of the Cu(II)-A $\beta$ (1-7)(OH) $_2^-$ ·PC adducts; (C) recurring molecular motifs in the adducts; (D–F) lowest energy, 4-coordinated, 5-coordinated (apical PO $_4$ ), and 5-coordinated (apical His6), respectively, along with their adduct binding energy.

The most stable form is four-coordinated (Figure 6D), as in free Cu(II)-A $\beta$ (1-7)(OH) $_2^-$ . The phosphate group in this structure forms two H-bond interactions (see Supplementary Materials, Table S2) with one OH of the Cu(II) coordination and one with the Arg5 side chain. The most stable five-coordinated form (+1.4 kcal/mol) has a phosphate group bound to Cu(II) in the apical position (Figure 6C, Cu-OP distance equal to 2.516 Å). Finally, the most stable five-coordinate form with apical His residue is 5.3 kcal/mol higher in energy (Figure 6F).

To investigate the thermochemistry of the OH propagation process, we considered three smaller Cu(II)-A $\beta$ (1-2)(OH) $_2^{\bullet-}$ ·PC model adducts. The most stable adduct is the one in which the quaternary ammonium portion forms three hydrogen bonds with Cu(II)-A $\beta$  (one with an OH ligand, one with Asp1 amino terminal, and one with the Asp1-Ala2 amide bond). The free binding energy is −2.9 kcal/mol. The structure with phosphate coordinated to Cu(II) in the apical position is 3.4 kcal/mol higher in energy.

The phosphocholine polar head group can be the target of OH radical propagation [47,48]. In the case of the PC moiety, three sites for OH attack via hydrogen abstraction reaction can be identified, namely the methyl groups at the quaternary ammonium and the *sn*-3 CH $_2$  and *sn*-2 CH glycerol backbone positions (Figure 5). In all possible scenarios, OH radical propagates with the formation of alkyl radicals, which are reactive species

susceptible to further radical propagation. According to Ref. [48], one possibility is that a second reduction equivalent reduces the radical carbon with the detachment of a portion of the phosphocholine. This latter step would result in the general destabilization of the phosphocholine unit, increasing the plasticity of the membrane and inducing damage (Figure 7).

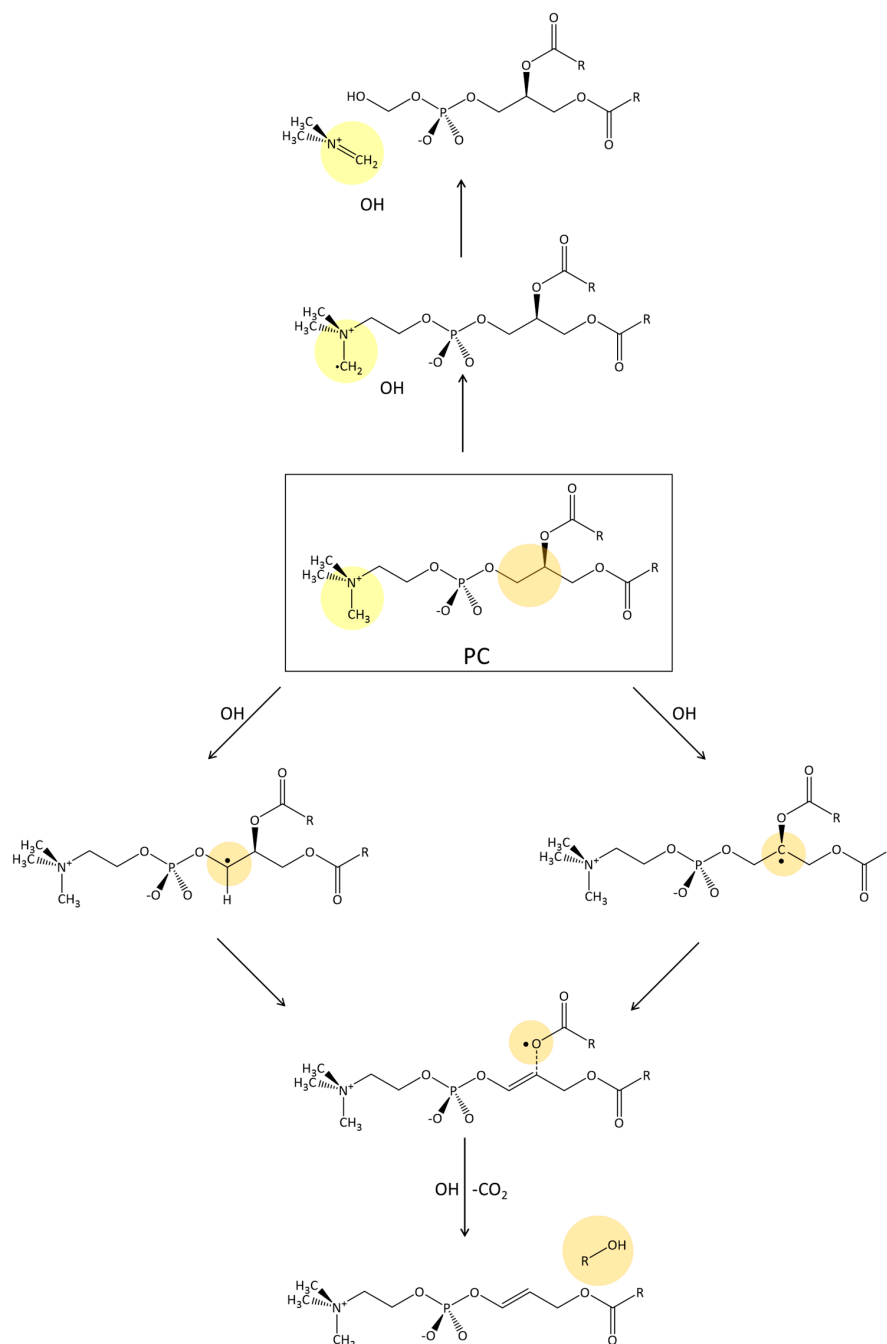


**Figure 7.** OH propagation reaction mechanisms toward the phosphocholine (PC) head group at the methyl of the quaternary ammonium portion or at the *sn*-3 CH<sub>2</sub>/*sn*-2 CH group of the glycerol portion (according to Ref. [48]). In all three cases, the first step is the H atom abstraction with the propagation of radical vacancy on the PC unit and the formation of a water molecule. In the case of attack at the quaternary ammonium, a second OH radical induces the detachment of NC<sub>3</sub>H<sub>8</sub><sup>+</sup> dimethylaminomethylene iminium cation and the formation of a hydroxyl group. In the case of attack at the glycerol unit, the formation of a C=C double bond induces the detachment of a CO<sub>2</sub> molecule; finally, the attack of a second OH brings to the formation of an alcohol.

Binding, activation, and reaction free energies for each adduct are reported in Table 1, while the scans of singlet and triplet PESs along the radical propagation coordinate are reported in Figure 8.

**Table 1.** Molecular interaction and radical propagation for the Cu(II)·Aβ·(OH)<sub>2</sub>•<sup>−</sup>·PC models and fatty acid chains for 4C and 5C. Binding, activation, and reaction free energy differences ( $\Delta G_b$ ,  $\Delta G^\ddagger$ , and  $\Delta G_r$ , respectively) are in kcal/mol.

Cu(II) Coordination	Attack Site	$\Delta G_b$	$\Delta G^\ddagger$	$\Delta G_r$
4C	N-CH <sub>3</sub>	−2.9	26.9	22.8
	CH <sub>2</sub>	6.8	23.6	5.3
	CH	3.7	15.1	6.9
5C	CH	0	15.9	−1.2
4C	16:0	8.5	16.6	16.2
	18:1	6.3	11.7	−1.4
	18:2	4.5	2.7	−15.4
5C	16:0	11.4	10.6	11.1

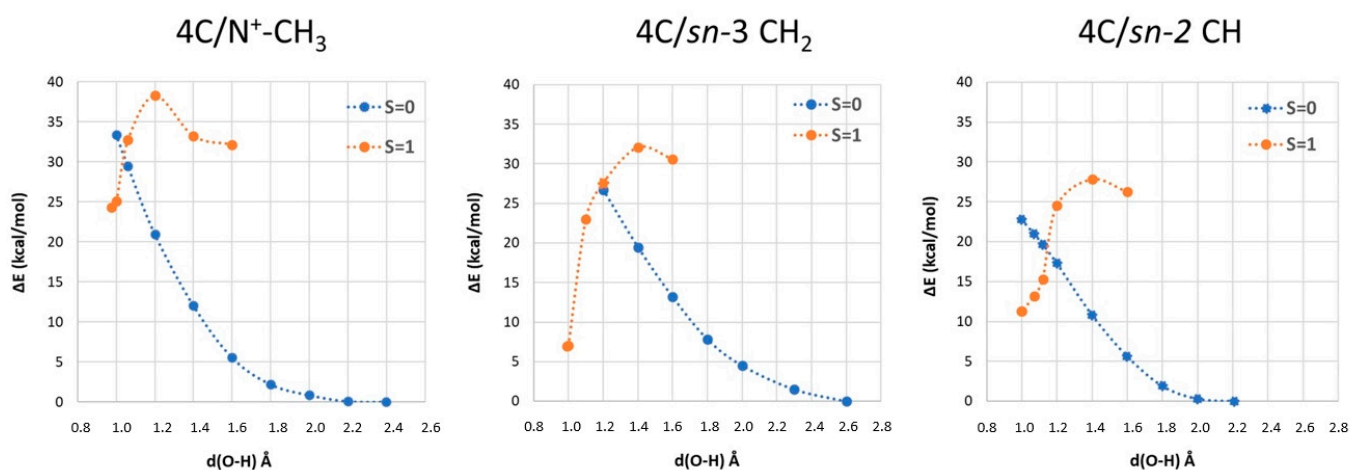
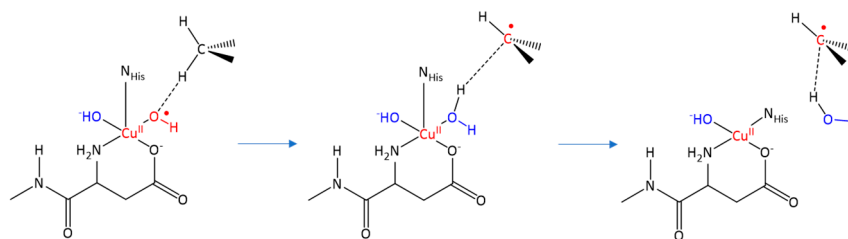


**Figure 8.** S = 0 and S = 1 PES scanning along the approaching coordinate between the oxygen atom of the OH, coordinated to Cu(II), and the H atom that belongs to the aliphatic carbon atom of the quaternary ammonium group (N<sup>+</sup>-CH<sub>3</sub>), and the CH<sub>2</sub> *sn*-3 and the CH *sn*-2 of the glycerol portion. 4C refers to the 4-coordinated Cu(II)·Aβ(1-2)·(OH)<sub>2</sub>•<sup>−</sup> model. The scan for 5C is reported in the Supplementary Materials. Distances in Å, total energy differences in kcal/mol. For each scan, the corresponding free energies (binding, barrier, and reaction) are reported in Table 1.

Upon hydrogen abstraction, the final product is the Cu(II)·Aβ·(H<sub>2</sub>O)(OH)<sup>−</sup>·PC• adduct in which the OH radical is reduced to a water molecule, leaving a radical carbon on the oxidized PC. The Cu atomic charges are slightly reduced upon H abstraction (on average, 1.20 e) with two unpaired electrons localized on the radical carbon atom and on the metal ion (see Figure S5 in Supplementary Materials). The S = 0 broken-symmetry and S = 1 solutions are very close in energy. The propagation toward CH *sn*-2 implies an activation free energy barrier of 15.1 kcal/mol, which makes this process chemically feasible. Oxidation of CH<sub>2</sub> *sn*-3 and quaternary ammonium groups are much less favorable, with activation barriers of 23.6 and 26.9 kcal/mol, respectively.

In the case of the propagation toward the CH *sn*-2 group, we investigated the reactivity of the 5C coordination (see Figure S7 in Supplementary Materials) with the aim of elucidating the influence of the fifth His ligand on the reaction free energy, according to the following mechanism:



where after OH propagation, the H<sub>2</sub>O ligand leaves the Cu(II) coordination sphere with the formation of a four-coordinated form. Here, the activation barrier does not change significantly (+0.8 kcal/mol), but the  $\Delta G_r$  value decreases by 8.1 kcal/mol.

#### 2.4. Fatty Acid Aliphatic Chains, Structure, and Reactivity toward Cu(II)-A $\beta$ -OH

In this section, we report the results of the reactivity of the Cu(II)·A $\beta$ ·(OH)<sub>2</sub><sup>•−</sup> models toward the saturated and polyunsaturated fatty acid chains considering the first step of lipid peroxidation [49], an oxidative chain reaction responsible for membrane damage induced by oxidative stress. The first step of this process is the hydrogen abstraction from a methylene C-H bond adjacent to the carbon–carbon double bond (monoallylic or bis-allylic position), especially in polyunsaturated fatty acids. Upon hydrogen abstraction by OH, a secondary CH<sup>•</sup> radical is formed, which then further propagates in the presence of an oxygen molecule, yielding various products, including highly reactive electrophilic aldehydes (such as malondialdehyde and 4-hydroxynonenal) [50,51].

We considered the methyl ester of three fatty acids, reported in Figure 9, chosen on the basis of the lipid raft composition (in mole %) of the human frontal brain cortex in AD patients [52] (16:0 is present at 23.6%, 18:1 ( $\omega$ -9) at 15.2% and 18:1 ( $\omega$ -6) at 0.8%).

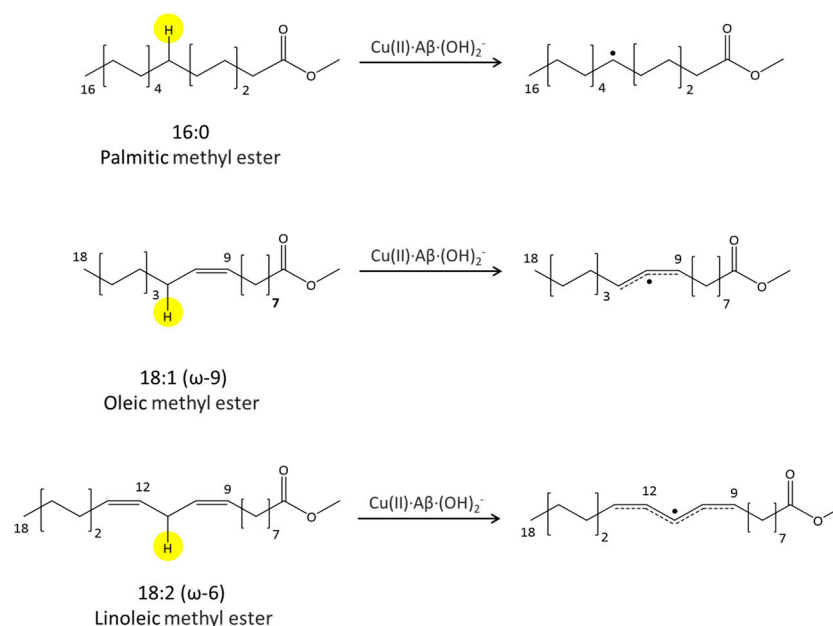


**Figure 9.** The structure of the three-fatty-acid methyl ester considered in this paper to model the initial step of the lipid peroxidation process in the presence of Cu(II)·A $\beta$ ·(OH)<sub>2</sub><sup>•−</sup>. The 16:0 chain is not the target of the lipid peroxidation but it allows a direct comparison of the oxidation power of OH coordinated to Cu(II) vs. free OH species; in 18:1 and 18:2, the attacks to the allylic and bis-allylic CH<sub>2</sub> positions are considered, respectively, with the formation of an allyl and a pentadienyl radical species.

The Cu(II)·A $\beta$ ·(OH)<sub>2</sub><sup>•−</sup> fatty acid adducts (see Figure S4 in Supplementary Materials) have been generated by searching the minimum energy structure in which the OH ligand on Cu(II) approached the hydrogen atom of the C-H under attack. All the structures

considered are characterized by a hydrogen bond between the ligand coordinated to Cu(II) and the carbonyl of the ester group, but the binding is not favored by 7.6 kcal/mol on average. The singlet and triplet PES scans along the OH propagation coordinates are reported in Figure 10.

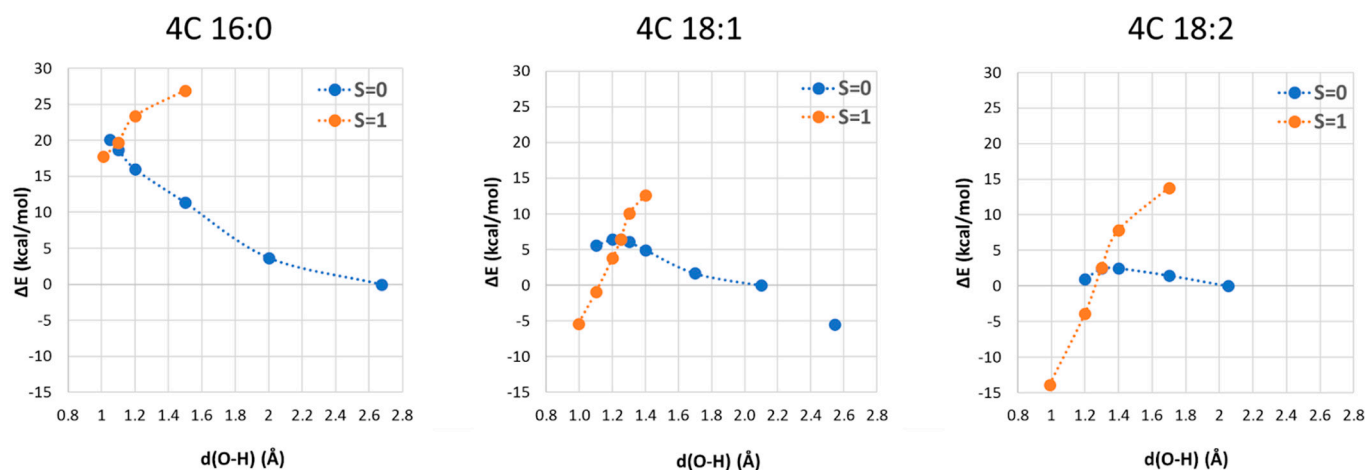


**Figure 10.** S = 0 and S = 1 PES scanning along the approaching coordinate between the oxygen atom of the OH, coordinated to Cu(II), and the H atom that belong to a CH<sub>2</sub> group of the fatty acid methyl ester aliphatic chain (see Figure 9). 4C refers to the 4-coordinated Cu(II)·Aβ·(OH)<sub>2</sub><sup>•−</sup> portion. Distances in Å, total energy differences in kcal/mol. For each scan, the corresponding binding barrier and reaction free energies are reported in Table 1.

By increasing the unsaturation number, we observed that the transition state structure becomes closer to the initial reactant (increasing the O···H distance), and consequently, the free energy barrier decreases. For 16:0, we compute a free energy barrier of 16.6 kcal/mol, suggesting that the attack toward a saturated fatty acid chain is still chemically feasible although slow, while for 18:1 and 18:2, the barriers are lower (11.7 and 2.7 kcal/mol, respectively), so these processes are much faster. The case of 18:1 is peculiar. Along the coordinates, we found a second local minimum higher in energy compared to the first one by 5.5 kcal/mol. The final product is the Cu(II)·Aβ·(H<sub>2</sub>O)(OH)<sup>−</sup>·(C•H) adduct in which the OH radical is reduced to a water molecule, leaving a secondary carbon radical on the aliphatic chain.

In the case of 18:1 and 18:2, we observe the formation of allylic and bis-allylic radicals, respectively, which stabilize the final product by resonance. S = 1 and broken symmetry S = 0 states are very close in energy. The copper ion is still in a Cu(II) redox state, with one unpaired electron localized on the radical carbon atom and the other on the copper ion (see Figure S6 in Supplementary Materials).

We finally considered the comparison between 4C and 5C coordination in the case of the 16:0 moiety (see Figure S8 in Supplementary Materials), as in the case of the PC oxidation pathways reported above. Starting from 5C coordination, the H abstraction process is thermodynamically and kinetically more favored ( $\Delta G^\ddagger$  and  $\Delta G_r$  decrease by 6.0 and 5.1 kcal/mol, respectively).

### 3. Discussion and Conclusions

The DFT modeling proposed led to a picture of the OH reactivity toward phospholipid oxidation that reveals new and interesting aspects.

The approach of PC moiety to Cu(II)·Aβ·OH coordination has been investigated using the Cu(II)·Aβ(1-7)·(OH)<sub>2</sub><sup>•−</sup> model, observing that the phosphate group is very likely to form an ion–ion interaction with the positively charged side chain of Arg5 or a Cu–OPO<sub>3</sub> bond. These interactions stabilize the adducts between PC and copper OH amyloid coordination, and the Cu–OPO<sub>3</sub> one could contribute to the broadening of the <sup>31</sup>P

NMR spectra observed by Gehman et al. [53] in model membranes associated with copper A $\beta$  complexes.

We investigated the OH propagation toward three possible sites of a phosphatidylcholine model (Figure 5) and toward the aliphatic chain of three fatty acids with increasing unsaturation (Figures 7 and 9). Once Cu(II)·A $\beta$ ·(OH) $_2^{\bullet-}$  has reached the PC, only the hydrogen abstraction at *sn*-2 CH is viable ( $\Delta G^\ddagger = 15.9$  kcal/mol) due to the formation of a more stable tertiary radical—CH $_2$ -C $\bullet$ -CH $_2$ -, and when 5C coordination is involved, the process is also slightly exergonic.

Next, we considered the hydrogen atom abstraction from one saturated and two unsaturated fatty acid aliphatic chains (Figure 9). We observed that the  $\Delta G^\ddagger$  decreases almost linearly with the increase in unsaturation, due to the higher stability of the allyl and then pentadienyl radicals. Remarkably, saturated fatty acid chains are not the target of lipid peroxidation, but the computation of  $\Delta G^\ddagger$  for 16:0 is a precise estimation of the Cu(II)·A $\beta$ ·(OH) $_2^{\bullet-}$  less oxidizing power (see Figure S9 in Supplementary Materials), a fact that also implies that Cu(II)-A $\beta$ -OH propagation processes are slower than those induced by solvated OH.

Also noteworthy is that if on the one hand, Cu(II)·A $\beta$  is a protective agent against radical species, on the other hand, it is also paradoxically able to increase the lifetime of the OH radicals and thus increase the risk of oxidative damage at the cellular level. Indeed, Cu(II)·A $\beta$  has a sort of redox neuroprotective system since it is less efficient in OH production than the free Cu(II) in solution. At the same time, Cu(II)·A $\beta$ ·(OH) $_2^{\bullet-}$  is less oxidant than free OH but it is still a sufficiently strong oxidant to induce oxidative stress. In particular, it has a much longer lifetime, allowing it to diffuse into the cell membrane lipid bilayer, where it starts lipid peroxidation. These results can also be seen in the context of the mechanism of A $\beta$  neurotoxicity. It has recently been proposed that the A $\beta$  small oligomers may penetrate [54] and aggregate within the membrane, forming unregulated and heterogeneous ion channels [55–57] which would allow ion dyshomeostasis [58], leading to cellular degeneration. In this context, it is useful to remind the reader that numerous studies [59–61] underline the important role of neuronal Ca $^{2+}$  dyshomeostasis in AD. A recent investigation [62] showed that oxidized membranes are prone to form native and oxidized domains which can induce a poration process [63]. In the hypothesis of an active role of Cu-A $\beta$ -OH in the oxidation of the neuronal membrane, as suggested by our simulations, this would favor the poration and therefore the dyshomeostasis of calcium.

In conclusion, the understanding of the molecular mechanism of Cu-A $\beta$  ROS production and propagation is crucial in the perspective of a better comprehension of AD etiology and hopefully for a therapeutic strategy.

It is well established that Cu(II)-A $\beta$  is redox-active and catalyzes the formation of OH coordinated to the metal ion. OH radicals produced by Cu(II)-A $\beta$  are added to those normally produced at the cellular level [64] but most likely in the extracellular area. Since OH radicals coordinated to Cu(II)-A $\beta$  have an attenuated redox potential, one may wonder if they can attack cell membranes by radical propagation. DFT investigation of such reactivity suggests that Cu(II)-A $\beta$ -OH can attack the *sn*-2 CH of the phosphocholine polar head and the mono- and bis-unsaturated fatty acid chains on a slower time scale compared to the free solvated OH radical. We can then infer that the Cu(II)-A $\beta$ -OH structure described in this paper could be one of the copper A $\beta$  species responsible for oxidative stress in AD.

#### 4. Computational Details

The DFT computations were performed using the pure GGA BP86 [65,66] DFT functional and RI technique [67], as implemented in TURBOMOLE [68]. Basis sets of triple- $\zeta$  plus polarization split valence quality [69] (def2-TZVP) were adopted for all atoms. The solvent effect was accounted for by using the COSMO (Conductor-like Screening Model) approach [70]. Water solvation was considered by setting the dielectric constant equal to 80 in the investigation of the PC reactivity. In the case of fatty acids, we considered a dielectric constant value of 4, thus mimicking the interior of a membrane. More in general,

this computational setting provides ground-state geometry parameters in good agreement with experimental X-ray values [71]. Charge distribution was evaluated using natural bond orbital analysis (NBO). Ground-state geometry optimizations were carried out with convergence criteria fixed to  $10^{-6}$  hartree for the energy and 0.001 hartree bohr for the gradient norm vector. For investigation of the fatty acid chain oxidation, D3 Grimme empirical dispersion correction [72] was adopted. The effects of ZPE, thermal, and entropic contributions on the purely electronic total energy values to compute free energies were investigated by means of evaluation of the approximated roto-translational partition function of each molecular species, at  $T = 298$  K and  $P = 1$  bar.

**Supplementary Materials:** The following supporting information can be downloaded at: <https://www.mdpi.com/article/10.3390/inorganics11060227/s1>, Table S1: DFT speciation of  $\text{Cu(II)(OH)}_2^- \cdot \text{A}\beta(1-7)$ ; Table S2–Figure S3:  $\text{Cu(II)(OH)}_2^- \cdot \text{A}\beta(1-7) \cdot \text{PC}$ ; Figure S4: Structures of the  $\text{Cu(II)(OH)}_2^- \cdot \text{A}\beta(1-2)$  fatty acid chain adducts; Figures S5 and S6: NBO spin population of the final products;  $\text{Cu(II)(OH)}_2^- \cdot \text{A}\beta(1-2) \cdot \text{PC}$  PES scans for 4C and 5C coordination; Figures S7–S9: Reactivity of free OH radical with 16:0 palmitic acid.

**Author Contributions:** L.B., F.A., L.D.G., J.V. and G.Z. designed the simulations; A.R. and L.C. performed the simulations; L.B., A.R. and L.C. analyzed the results; L.B. and F.A. wrote the manuscript. All authors have read and agreed to the published version of the manuscript.

**Funding:** This work was supported by the PRIN Project 2020BKK3W9.

**Data Availability Statement:** Not applicable.

**Conflicts of Interest:** The authors declare no conflict of interest.

## References

1. Alzheimer's Association. 2022 Alzheimer's Disease Facts and Figures. *Alzheimers. Dement.* **2022**, *18*, 700–789. [CrossRef]
2. Hardy, J.A.; Higgins, G.A. Alzheimer's Disease: The Amyloid Cascade Hypothesis. *Science* **1992**, *256*, 184–185. [CrossRef]
3. Budd Haeberlein, S.; Aisen, P.S.; Barkhof, F.; Chalkias, S.; Chen, T.; Cohen, S.; Dent, G.; Hansson, O.; Harrison, K.; von Hehn, C.; et al. Two Randomized Phase 3 Studies of Aducanumab in Early Alzheimer's Disease. *J. Prev. Alzheimers Dis.* **2022**, *9*, 197–210. [CrossRef]
4. Makin, S. The Amyloid Hypothesis on Trial. *Nature* **2018**, *559*, S4–S7. [CrossRef]
5. Doig, A.J.; del Castillo-Frias, M.P.; Berthoumieu, O.; Tarus, B.; Nasica-Labouze, J.; Sterpone, F.; Nguyen, P.H.; Hooper, N.M.; Faller, P.; Derreumaux, P. Why Is Research on Amyloid Failing to Give New Drugs for Alzheimers Disease? *ACS Chem. Neurosci.* **2017**, *8*, 1435–1437. [CrossRef]
6. Lei, P.; Ayton, S.; Bush, A.I. The Essential Elements of Alzheimer's Disease. *J. Biol. Chem.* **2021**, *296*, 100105. [CrossRef]
7. Ayton, S.; Bush, A.I.  $\beta$ -Amyloid: The Known Unknowns. *Ageing Res. Rev.* **2021**, *65*, 101212. [CrossRef]
8. Abelein, A.; Abrahams, J.P.; Danielsson, J.; Gräslund, A.; Jarvet, J.; Luo, J.; Tiiman, A.; Wärmländer, S.K.T.S. The Hairpin Conformation of the Amyloid  $\beta$  Peptide Is an Important Structural Motif along the Aggregation Pathway. *J. Biol. Inorg. Chem.* **2014**, *19*, 623–634. [CrossRef]
9. Cline, E.N.; Bicca, M.A.; Viola, K.L.; Klein, W.L. The Amyloid- $\beta$  Oligomer Hypothesis: Beginning of the Third Decade. *J. Alzheimer's Dis.* **2018**, *64*, S567–S610. [CrossRef]
10. Michaels, T.C.T.; Šarić, A.; Curk, S.; Bernfur, K.; Arosio, P.; Meisl, G.; Dear, A.J.; Cohen, S.I.A.; Dobson, C.M.; Vendruscolo, M.; et al. Author Correction: Dynamics of Oligomer Populations Formed during the Aggregation of Alzheimer's A $\beta$ 42 Peptide. *Nat. Chem.* **2020**, *12*, 497. [CrossRef]
11. Nguyen, P.H.; Ramamoorthy, A.; Sahoo, B.R.; Zheng, J.; Faller, P.; Straub, J.E.; Dominguez, L.; Shea, J.-E.; Dokholyan, N.V.; De Simone, A.; et al. Amyloid Oligomers: A Joint Experimental/Computational Perspective on Alzheimer's Disease, Parkinson's Disease, Type II Diabetes, and Amyotrophic Lateral Sclerosis. *Chem. Rev.* **2021**, *121*, 2545–2647. [CrossRef]
12. Squitti, R.; Faller, P.; Hureau, C.; Granzotto, A.; White, A.R.; Kepp, K.P. Copper Imbalance in Alzheimer's Disease and Its Link with the Amyloid Hypothesis: Towards a Combined Clinical, Chemical, and Genetic Etiology. *J. Alzheimers. Dis.* **2021**, *83*, 23–41. [CrossRef]
13. Lovell, M.A.; Robertson, J.D.; Teesdale, W.J.; Campbell, J.L.; Markesbery, W.R. Copper, Iron and Zinc in Alzheimer's Disease Senile Plaques. *J. Neurol. Sci.* **1998**, *158*, 47–52. [CrossRef]
14. Atrián-Blasco, E.; Gonzalez, P.; Santoro, A.; Alias, B.; Faller, P.; Hureau, C. Cu and Zn Coordination to Amyloid Peptides: From Fascinating Chemistry to Debated Pathological Relevance. *Coord. Chem. Rev.* **2018**, *375*, 38–55. [CrossRef]
15. Atrián-Blasco, E.; Cerrada, E.; Conte-Daban, A.; Testemale, D.; Faller, P.; Laguna, M.; Hureau, C. Copper(I) Targeting in the Alzheimer's Disease Context: A First Example Using the Biocompatible PTA Ligand. *Metallomics* **2015**, *7*, 1229–1232. [CrossRef]

16. Faller, P.; Hureau, C. A Bioinorganic View of Alzheimer's Disease: When Misplaced Metal Ions (Re)direct the Electrons to the Wrong Target. *Chem. Eur. J.* **2012**, *18*, 15910–15920. [[CrossRef](#)]
17. Pardo-Moreno, T.; González-Acedo, A.; Rivas-Domínguez, A.; García-Morales, V.; García-Cozar, F.J.; Ramos-Rodríguez, J.J.; Melguizo-Rodríguez, L. Therapeutic Approach to Alzheimer's Disease: Current Treatments and New Perspectives. *Pharmaceutics* **2022**, *14*, 1117. [[CrossRef](#)]
18. Dong, J.; Atwood, C.S.; Anderson, V.E.; Siedlak, S.L.; Smith, M.A.; Perry, G.; Carey, P.R. Metal Binding and Oxidation of Amyloid-Beta within Isolated Senile Plaque Cores: Raman Microscopic Evidence. *Biochemistry* **2003**, *42*, 2768–2773. [[CrossRef](#)]
19. Greenough, M.A.; Camakaris, J.; Bush, A.I. Metal Dyshomeostasis and Oxidative Stress in Alzheimer's Disease. *Neurochem. Int.* **2013**, *62*, 540–555. [[CrossRef](#)]
20. Kepp, K.P.; Squitti, R. Copper Imbalance in Alzheimer's Disease: Convergence of the Chemistry and the Clinic. *Coord. Chem. Rev.* **2019**, *397*, 168–187. [[CrossRef](#)]
21. Bradley, M.A.; Xiong-Fister, S.; Markesbery, W.R.; Lovell, M.A. Elevated 4-Hydroxyhexenal in Alzheimer's Disease (AD) Progression. *Neurobiol. Aging* **2012**, *33*, 1034–1044. [[CrossRef](#)]
22. Butterfield, D.A.; Reed, T.; Perluigi, M.; De Marco, C.; Coccia, R.; Cini, C.; Sultana, R. Elevated Protein-Bound Levels of the Lipid Peroxidation Product, 4-Hydroxy-2-Nonenal, in Brain from Persons with Mild Cognitive Impairment. *Neurosci. Lett.* **2006**, *397*, 170–173. [[CrossRef](#)]
23. Collin, F. Chemical Basis of Reactive Oxygen Species Reactivity and Involvement in Neurodegenerative Diseases. *Int. J. Mol. Sci.* **2019**, *20*, 2407. [[CrossRef](#)]
24. Butterfield, D.A.; Halliwell, B. Oxidative Stress, Dysfunctional Glucose Metabolism and Alzheimer Disease. *Nat. Rev. Neurosci.* **2019**, *20*, 148–160. [[CrossRef](#)]
25. Cheignon, C.; Tomas, M.; Bonnefont-Rousselot, D.; Faller, P.; Hureau, C.; Collin, F. Oxidative Stress and the Amyloid Beta Peptide in Alzheimer's Disease. *Redox Biol.* **2018**, *14*, 450–464. [[CrossRef](#)]
26. Furlan, S.; Hureau, C.; Faller, P.; La Penna, G. Modeling Copper Binding to the Amyloid- $\beta$  Peptide at Different pH: Toward a Molecular Mechanism for Cu Reduction. *J. Phys. Chem. B* **2012**, *116*, 11899–11910. [[CrossRef](#)]
27. Singh, S.K.; Balendra, V.; Obaid, A.A.; Esposito, J.; Tikhonova, M.A.; Gautam, N.K.; Poeggeler, B. Copper-Mediated  $\beta$ -Amyloid Toxicity and Its Chelation Therapy in Alzheimer's Disease. *Metallomics* **2022**, *14*, mfac018. [[CrossRef](#)]
28. Mutter, S.T.; Turner, M.; Deeth, R.J.; Platts, J.A. Metal Binding to Amyloid- $\beta$ : A Ligand Field Molecular Dynamics Study. *ACS Chem. Neurosci.* **2018**, *9*, 2795–2806. [[CrossRef](#)]
29. Rauk, A. The Chemistry of Alzheimer's Disease. *Chem. Soc. Rev.* **2009**, *38*, 2698–2715. [[CrossRef](#)]
30. Cheignon, C.; Collin, F.; Faller, P.; Hureau, C. Is Ascorbate Dr Jekyll or Mr Hyde in the Cu(A $\beta$ ) Mediated Oxidative Stress Linked to Alzheimer's Disease? *Dalton Trans.* **2016**, *45*, 12627–12631. [[CrossRef](#)]
31. Cheignon, C.; Jones, M.; Atrián-Blasco, E.; Kieffer, I.; Faller, P.; Collin, F.; Hureau, C. Identification of Key Structural Features of the Elusive Cu–A $\beta$  Complex That Generates ROS in Alzheimer's Disease. *Chem. Sci.* **2017**, *8*, 5107–5118. [[CrossRef](#)]
32. Reybier, K.; Ayala, S.; Alies, B.; Rodrigues, J.V.; Bustos Rodriguez, S.; La Penna, G.; Collin, F.; Gomes, C.M.; Hureau, C.; Faller, P. Free Superoxide Is an Intermediate in the Production of H<sub>2</sub>O<sub>2</sub> by Copper(I)-A $\beta$  Peptide and O<sub>2</sub>. *Angew. Chem. Int. Ed. Engl.* **2016**, *55*, 1085–1089. [[CrossRef](#)]
33. Cassagnes, L.-E.; Hervé, V.; Nepveu, F.; Hureau, C.; Faller, P.; Collin, F. The Catalytically Active Copper-Amyloid-Beta State: Coordination Site Responsible for Reactive Oxygen Species Production. *Angew. Chem. Int. Ed. Engl.* **2013**, *52*, 11110–11113. [[CrossRef](#)]
34. La Penna, G.; Hureau, C.; Andreussi, O.; Faller, P. Identifying, By First-Principles Simulations, Cu[Amyloid- $\beta$ ] Species Making Fenton-Type Reactions in Alzheimer's Disease. *J. Phys. Chem. B* **2013**, *117*, 16455–16467. [[CrossRef](#)]
35. Bradley-Whitman, M.A.; Timmons, M.D.; Beckett, T.L.; Murphy, M.P.; Lynn, B.C.; Lovell, M.A. Nucleic Acid Oxidation: An Early Feature of Alzheimer's Disease. *J. Neurochem.* **2014**, *128*, 294–304. [[CrossRef](#)]
36. Sultana, R.; Allan Butterfield, D. Oxidative Modification of Brain Proteins in Alzheimer's Disease: Perspective on Future Studies Based on Results of Redox Proteomics Studies. *J. Alzheimer's Dis.* **2012**, *33*, S243–S251. [[CrossRef](#)]
37. Butterfield, D.A.; Lauderback, C.M. Lipid Peroxidation and Protein Oxidation in Alzheimer's Disease Brain: Potential Causes and Consequences Involving Amyloid  $\beta$ -Peptide-Associated Free Radical Oxidative Stress. *Free. Radic. Biol. Med.* **2002**, *32*, 1050–1060. [[CrossRef](#)]
38. Butterfield, D.A.; Allan Butterfield, D.; Reed, T.; Newman, S.F.; Sultana, R. Roles of Amyloid  $\beta$ -Peptide-Associated Oxidative Stress and Brain Protein Modifications in the Pathogenesis of Alzheimer's Disease and Mild Cognitive Impairment. *Free Radic. Biol. Med.* **2007**, *43*, 658–677. [[CrossRef](#)]
39. Peña-Bautista, C.; Tirlé, T.; López-Nogueroles, M.; Vento, M.; Baquero, M.; Cháfer-Pericás, C. Oxidative Damage of DNA as Early Marker of Alzheimer's Disease. *Int. J. Mol. Sci.* **2019**, *20*, 6136. [[CrossRef](#)]
40. Nasica-Labouze, J.; Nguyen, P.H.; Sterpone, F.; Berthoumieu, O.; Buchete, N.-V.; Coté, S.; De Simone, A.; Doig, A.J.; Faller, P.; Garcia, A.; et al. Amyloid  $\beta$  Protein and Alzheimer's Disease: When Computer Simulations Complement Experimental Studies. *Chem. Rev.* **2015**, *115*, 3518–3563. [[CrossRef](#)]
41. Strodel, B.; Coskuner-Weber, O. Transition Metal Ion Interactions with Disordered Amyloid- $\beta$  Peptides in the Pathogenesis of Alzheimer's Disease: Insights from Computational Chemistry Studies. *J. Chem. Inf. Model.* **2019**, *59*, 1782–1805. [[CrossRef](#)]

42. Giacobazzi, R.; Ciofini, I.; Rao, L.; Amatore, C.; Adamo, C. Copper-amyloid- $\beta$  Complex May Catalyze Peroxynitrite Production in Brain: Evidence from Molecular Modeling. *Phys. Chem. Chem. Phys.* **2014**, *16*, 10169–10174. [[CrossRef](#)]
43. Prosdocimi, T.; De Gioia, L.; Zampella, G.; Bertini, L. On the Generation of OH( $\cdot$ ) Radical Species from H<sub>2</sub>O<sub>2</sub> by Cu(I) Amyloid Beta Peptide Model Complexes: A DFT Investigation. *J. Biol. Inorg. Chem.* **2016**, *21*, 197–212. [[CrossRef](#)]
44. Arrigoni, F.; Prosdocimi, T.; Mollica, L.; De Gioia, L.; Zampella, G.; Bertini, L. Copper Reduction and Dioxygen Activation in Cu-Amyloid Beta Peptide Complexes: Insight from Molecular Modelling. *Metallomics* **2018**, *10*, 1618–1630. [[CrossRef](#)]
45. Arrigoni, F.; Di Carlo, C.; Rovetta, A.; De Gioia, L.; Zampella, G.; Bertini, L. Superoxide Reduction by Cu-Amyloid Beta Peptide Complexes: A Density Functional Theory Study. *Eur. J. Inorg. Chem.* **2022**, *2022*, e202200245. [[CrossRef](#)]
46. Arrigoni, F.; Rizza, F.; Tisi, R.; De Gioia, L.; Zampella, G.; Bertini, L. On the Propagation of the OH Radical Produced by Cu-Amyloid Beta Peptide Model Complexes. *Insight Mol. Modelling Met.* **2020**, *12*, 1765–1780.
47. Maciel, E.; da Silva, R.N.; Simões, C.; Domingues, P.; Domingues, M.R.M. Structural Characterization of Oxidized Glycerophosphatidylserine: Evidence of Polar Head Oxidation. *J. Am. Soc. Mass. Spectrom.* **2011**, *22*, 1804–1814. [[CrossRef](#)]
48. Yusupov, M.; Wende, K.; Kupsch, S.; Neyts, E.C.; Reuter, S.; Bogaerts, A. Effect of Head Group and Lipid Tail Oxidation in the Cell Membrane Revealed through Integrated Simulations and Experiments. *Sci. Rep.* **2017**, *7*, 5761. [[CrossRef](#)]
49. Yin, H.; Xu, L.; Porter, N.A. Free Radical Lipid Peroxidation: Mechanisms and Analysis. *Chem. Rev.* **2011**, *111*, 5944–5972. [[CrossRef](#)]
50. Barrera, G.; Pizzimenti, S.; Daga, M.; Dianzani, C.; Arcaro, A.; Cetrangolo, G.P.; Giordano, G.; Cucci, M.A.; Graf, M.; Gentile, F. Lipid Peroxidation-Derived Aldehydes, 4-Hydroxynonenal and Malondialdehyde in Aging-Related Disorders. *Antioxidants* **2018**, *7*, 102. [[CrossRef](#)]
51. Solís-Calero, C.; Ortega-Castro, J.; Frau, J.; Muñoz, F. Nonenzymatic Reactions above Phospholipid Surfaces of Biological Membranes: Reactivity of Phospholipids and Their Oxidation Derivatives. *Oxid. Med. Cell. Longev.* **2015**, *2015*, 319505. [[CrossRef](#)] [[PubMed](#)]
52. Martín, V.; Fabelo, N.; Santpere, G.; Puig, B.; Marín, R.; Ferrer, I.; Díaz, M. Lipid Alterations in Lipid Rafts from Alzheimer's Disease Human Brain Cortex. *J. Alzheimers. Dis.* **2010**, *19*, 489–502. [[CrossRef](#)] [[PubMed](#)]
53. Gehman, J.D.; O'Brien, C.C.; Shabanpoor, F.; Wade, J.D.; Separovic, F. Metal Effects on the Membrane Interactions of Amyloid- $\beta$  Peptides. *Eur. Biophys. J.* **2008**, *37*, 333–344. [[CrossRef](#)] [[PubMed](#)]
54. Lockhart, C.; Klimov, D.K. Alzheimer's A $\beta$ 10–40 Peptide Binds and Penetrates DMPC Bilayer: An Isobaric-Isothermal Replica Exchange Molecular Dynamics Study. *J. Phys. Chem. B.* **2014**, *118*, 2638–2648. [[CrossRef](#)] [[PubMed](#)]
55. Sciacca, M.F.M.; Kotler, S.A.; Brender, J.R.; Chen, J.; Lee, D.-K.; Ramamoorthy, A. Two-Step Mechanism of Membrane Disruption by A $\beta$  through Membrane Fragmentation and Pore Formation. *Biophys. J.* **2012**, *103*, 702–710. [[CrossRef](#)]
56. Jang, H.; Zheng, J.; Nussinov, R. Models of  $\beta$ -Amyloid Ion Channels in the Membrane Suggest That Channel Formation in the Bilayer Is a Dynamic Process. *Biophys. J.* **2007**, *93*, 1938–1949. [[CrossRef](#)]
57. Sepehri, A.; Lazaridis, T. Putative Structures of Membrane-Embedded Amyloid  $\beta$  Oligomers. *ACS Chem. Neurosci.* **2023**, *14*, 99–110. [[CrossRef](#)]
58. Supnet, C.; Bezprozvanny, I. The Dysregulation of Intracellular Calcium in Alzheimer Disease. *Cell. Calcium* **2010**, *47*, 183–189. [[CrossRef](#)]
59. LaFerla, F.M. Calcium Dyshomeostasis and Intracellular Signalling in Alzheimer's Disease. *Nat. Rev. Neurosci.* **2002**, *3*, 862–872. [[CrossRef](#)]
60. Kawahara, M.; Negishi-Kato, M.; Sadakane, Y. Calcium Dyshomeostasis and Neurotoxicity of Alzheimer's  $\beta$ -Amyloid Protein. *Expert. Rev. Neurother.* **2009**, *9*, 681–693. [[CrossRef](#)]
61. Chami, M. Calcium Signalling in Alzheimer's Disease: From Pathophysiological Regulation to Therapeutic Approaches. *Cells* **2021**, *10*, 140. [[CrossRef](#)] [[PubMed](#)]
62. Oliveira, M.C.; Yusupov, M.; Bogaerts, A.; Cordeiro, R.M. Molecular Dynamics Simulations of Mechanical Stress on Oxidized Membranes. *Biophys. Chem.* **2019**, *254*, 106266. [[CrossRef](#)] [[PubMed](#)]
63. Haluska, C.K.; Baptista, M.S.; Fernandes, A.U.; Schroder, A.P.; Marques, C.M.; Itri, R. Photo-Activated Phase Separation in Giant Vesicles Made from Different Lipid Mixtures. *Biochim. Biophys. Acta* **2012**, *1818*, 666–672. [[CrossRef](#)] [[PubMed](#)]
64. Ayala, A.; Muñoz, M.F.; Argüelles, S. Lipid Peroxidation: Production, Metabolism, and Signaling Mechanisms of Malondialdehyde and 4-Hydroxy-2-Nonenal. *Oxid. Med. Cell. Longev.* **2014**, *2014*, 360438. [[CrossRef](#)] [[PubMed](#)]
65. Becke, A.D. Density-Functional Exchange-Energy Approximation with Correct Asymptotic Behavior. *Phys. Rev. A Gen. Phys.* **1988**, *38*, 3098–3100. [[CrossRef](#)]
66. Perdew, J.P. Density-Functional Approximation for the Correlation Energy of the Inhomogeneous Electron Gas. *Phys. Rev. B. Condens. Matter* **1986**, *33*, 8822–8824. [[CrossRef](#)]
67. Eichkorn, K.; Weigend, F.; Treutler, O.; Ahlrichs, R. Auxiliary Basis Sets for Main Row Atoms and Transition Metals and Their Use to Approximate Coulomb Potentials. *Theor. Chem. Acc.* **1997**, *97*, 119–124. [[CrossRef](#)]
68. Ahlrichs, R.; Bär, M.; Häser, M.; Horn, H.; Kölmel, C. Electronic Structure Calculations on Workstation Computers: The Program System Turbomole. *Chem. Phys. Lett.* **1989**, *162*, 165–169. [[CrossRef](#)]
69. Schäfer, A.; Huber, C.; Ahlrichs, R. Fully Optimized Contracted Gaussian Basis Sets of Triple Zeta Valence Quality for Atoms Li to Kr. *J. Chem. Phys.* **1994**, *100*, 5829–5835. [[CrossRef](#)]

70. Bertini, L.; Bruschi, M.; Romaniello, M.; Zampella, G.; Tiberti, M.; Barbieri, V.; Greco, C.; La Mendola, D.; Bonomo, R.P.; Fantucci, P.; et al. Copper Coordination to the Putative Cell Binding Site of Angiogenin: A DFT Investigation. In *Highlights in Theoretical Chemistry*; Springer: Berlin/Heidelberg, Germany, 2012; pp. 255–269.
71. Klamt, A.; Schüürmann, G. COSMO: A New Approach to Dielectric Screening in Solvents with Explicit Expressions for the Screening Energy and Its Gradient. *J. Chem. Soc. Perkin Trans.* **1993**, *2*, 799–805. [[CrossRef](#)]
72. Grimme, S. Semiempirical GGA-Type Density Functional Constructed with a Long-Range Dispersion Correction. *J. Comput. Chem.* **2006**, *27*, 1787–1799. [[CrossRef](#)] [[PubMed](#)]

**Disclaimer/Publisher’s Note:** The statements, opinions and data contained in all publications are solely those of the individual author(s) and contributor(s) and not of MDPI and/or the editor(s). MDPI and/or the editor(s) disclaim responsibility for any injury to people or property resulting from any ideas, methods, instructions or products referred to in the content.